Ionospheric Pc1 waves during a storm recovery phase observed by CSES

Xiaochen Gou[1], Lei Li[1*], Yiteng Zhang[1*], Bin Zhou[1], Yongyong Feng[1], Bingjun Cheng[1], Tero Raita[3], Ji Liu[1], ZhiMa Zeren[2], Xuhui Shen[2]

[1]State Key Laboratory of Space Weather, National Space Science Center, Chinese Academy of Sciences, Beijing, China;
[2]Institute of Crustal Dynamic, China Earthquake Administration, Beijing, China;
[3]Sodankylä Geophysical Observatory, University of Oulu, Sodankylä, Finland

Abstract

During the storm recovery phase on August 27, 2018, the China Seismo-Electromagnetic Satellite (CSES) detected Pc1 wave activities both in the Northern and Southern hemispheres in the high latitude post-midnight ionosphere with a central frequency about 2 Hz. Meanwhile, the typical Pc1 waves were simultaneously observed by the Sodankylä Geophysical Observatory (SGO) stations on the ground for several hours. In this paper, we study the propagation characteristics and possible source regions of those waves. Firstly, we find that the Pc1 waves observed by the satellites exhibited mixed polarization and the wave normal is almost parallel with the background magnetic field. The field-aligned Poynting fluxes point downward in both hemispheres, implying the satellites are close to the wave injection regions in the ionosphere at about *L*=3. Furthermore, we also find that the estimated position of the plasmapause calculated by models is almost at *L*=3. Therefore, we suggest the possible sources of waves are near the plasmapause, which is consistent with previous studies that the outward expansion of the plasmasphere into the ring current during the recovery phase of geomagnetic storms may generate electromagnetic ion cyclotron (EMIC) waves and then these EMIC waves propagate along the background magnetic field northward and southward to the ionosphere at about *L*=3. Additionally, the ground station data show that Pc1 wave power attenuates with increasing distance from *L*=3, supporting the idea that CSES observes the wave activities near the injection region. The observations are unique in that the Pc1 waves are observed in the ionosphere in nearly conjugate regions, where transvers Alfven waves propagate down into the ionosphere.

1 Introduction

Electromagnetic ion cyclotron (EMIC) waves are in the typical frequency range of 0.1–

5Hz which corresponds to Pc1 pulsations on the ground. Generally, in the magnetosphere, EMIC wave can be excited by cyclotron instability of hot ions (1-100 keV) with temperature anisotropy ($T_{\perp}>T_{//}$) near the Earth's magnetic equator, particularly, in the region with large plasma density and weak magnetic field, such as the plasmapause, ring current and plasma sheet [Cornwall et al., 1965; Erlandson et al.,1993; Horne and Thorne, 1993; Anderson et al., 1996; Lin et al., 2014]. Previous studies indicate that hot ion temperature anisotropy ($T_{\perp}>T_{//}$) near the Earth's magnetic equator can be caused by several possible mechanisms, such as plasmapause expanding into ring current region during storm recovery phase [Cornwall et al.,1970; Russell & Thorne, 1970], mid-energy ions penetrating into the ring current region from the plasma sheet [Bossen et al., 1976], the solar wind dynamic pressure enhancement or the magnetosphere compression [Olson & Lee, 1983; Anderson & Hamilton, 1993; McCollough et al., 2010; Usanova et al. 2012]. Statistical results show that EMIC waves are associated with increased magnetic activity and have a peak occurrence during the storm recovery phase [Wentworth, 1964; Erlandson & Ukhorskiy, 2001; Bortnik et al., 2008].

Generally, EMIC waves are excited at or near the Earth's magnetic equator, and then propagate along the background magnetic field toward the high latitude region, can penetrate into the upper ionosphere under certain conditions. The left-hand polarized (LHP) Alfvén waves incident from the magnetosphere can couple to the right-hand polarized (RHP) compressional, isotropic waves in the ionosphere by the anisotropic ionospheric Hall currents [Fraser et al., 1975a, 1975b; Fujita and Tamao 1988]. Since the wavelength of EMIC waves with frequency about 1Hz is comparable with the scale size of the ionospheric minimum in the Alfven speed, they can be trapped and ducted in this region of low Alfven speed [Lysak et al., 1999]. Thus, the EMIC waves can be observed both at the low earth orbit (LEO) and on the ground as Pc1 geomagnetic pulsations with different characteristics.

At ionospheric altitudes, satellite observations of Pc1 waves are usually provided by the onboard magnetometers. Magsat observed Pc1 waves at an ionospheric altitude of 350-550km, with both LH and RH polarizations in a latitudinally narrow (<100 km) region [Iyemori and Hayashi, 1989]. In recent years, with the development of LEO satellites, various statistical studies of EMIC waves have been carried out to reveal the global propagation characteristics, spatial distribution, and geomagnetic dependence of Pc1 waves. Since the field-aligned currents mask the Pc1 pulsations in the high latitude zone, excluding data at auroral latitudes , according to the statistical analysis of CHAMP satellite data during one solar cycle, Park et al. [2013] found that Pc1 waves

are mostly linearly polarized, having a peak occurrence at sub-auroral latitudes, and weakly dependent on magnetic activity and the solar wind velocity. Similarly, the Swarm data show a peak occurrence rate of Pc1 waves at middle latitude including sub-auroral region. Moreover, these waves are linear polarization dominated, propagating oblique to the background magnetic field, and preferably occur during the late recovery phase of magnetic storms [Kim et al. 2018a].

In this paper, we report a Pc1 wave event observed by the China Seismo-Electromagnetic Satellite (CSES), as well as the Swarm satellite. Based on both electric and magnetic field measurements, we study the propagation characteristics and possible source regions of those Pc1 waves occurring at high latitude in the Northern and Southern hemisphere ionosphere during the recovery phase of the geomagnetic storm on 25-28 August 2018.

2 Data sources

The China Seismo-Electromagnetic Satellite (CSES) was launched on February 2, 2018, into a sun-synchronous circular orbit at an altitude of 507 km with an inclination angle of 97.4°. The local time of the descending node is 14:00. We use the magnetic field data from the High Precision Magnetometer (HPM) and the electric field data from the Electric Field Detector (EFD) onboard CSES. HPM includes two three-components fluxgate sensors to collect vector magnetic field data with a sampling rate of 60Hz, and the noise of the sensors are less than 0.02nT /√Hz @1 Hz [Zhou et al., 2018; 2019]. EFD consists of four spherical sensors, which can realize three-components electric field detection at a broad frequency range from DC to 3.5MHz, in which the ULF band provides 125Hz sampled waveform signal [Huang et al., 2018]. Swarm was launched on November 22, 2013, which has three satellites (Alpha, Bravo, and Charlie) at altitudes of 450 – 550 km with an inclination angle of 88° [Friis-Christensen et al., 2006]. For this study, we used magnetic field data from Swarm A with a high sampling rate of 50 Hz and a noise level of 0.01 nT/√Hz @1Hz [Merayo, 2014]. We also use the Finnish pulsation magnetometers data from Sodankylä Geophysical Observatory (SGO) including Sodankylä (SOD), Oulu (OUL), and Nurmijärvi (NUR) with a sampling rate of 40 Hz. In addition, the solar wind data of OMNI is from CDA Web. The Dst index is from WDC Web and the plasmapause simulation data is from NASA CCMC Web.

3 Observations

Figure 1 shows the variation of solar wind parameters and the geomagnetic index during the Pc 1 wave event in this study. The Dst index, interplanetary magnetic field,

solar wind speed and solar wind dynamic pressure from Aug. 25 to 29, 2018 are shown from top to bottom. It can be seen that during the magnetic storm, the Dst index decreased to -170 nT at 8:00 26 August. The Pc1 waves were observed by CSES and Swarm between UTC 22:50 – 23:30 (marked by the black box in Figure 1) with northward interplanetary magnetic field (IMF) and minor increased Dst index in the magnetic storm recovery phase on Aug. 27, 2018.

3.1 Spatial-temporal characteristics of Pc1 waves

On Aug. 27, 2018, CSES and Swarm -A satellites passed through the ionospheric Pc1 wave regions for three times, in the Northern and Southern hemispheres, marked by squares (CSES) and triangles (Swarm) in Figure 2. Firstly, at around UTC 23:00 (local time about 02:06 to 02:34), Swarm -A and CSES satellites successively observed Pc1 waves in the Southern hemisphere at geomagnetic latitude about 56° S~53° S with *L* shell value about 3.0 ~ 3.4. The distance between the two satellites is about 300km. Swarm -A observed the Pc1 waves at about UTC 22:50 (QD-LAT=56° S, *L*=3.4) about 10 minutes before CSES, with a maximum amplitude about 12 nT and a central frequency about 2 Hz, lasting for 1 minute, as shown in Figure 3. Then, CSES observed the Pc1 wave at UTC 23:02 (QD-LAT=54°S, L=3.1) by the HPM Magnetometer (shown in Figure 4), with a maximum amplitude about 1.5 nT and a central frequency about 2 Hz, lasting a minute and a half. Thereafter, at about UTC 23:30 (local time about 01:27 to 01:22), the CSES flew away to the Northern hemisphere, passing through the Pc1 wave region again at geomagnetic latitudes about 54° N, *L* values about 3.1. As shown in Figure 5, the maximum amplitude is about 10 nT and the central frequency is about 2 Hz, with a duration about 1 minute. Around this time, since the Swarm satellite was about 6000 km northeast of the CSES satellite, no Pc1 waves were observed by Swarm.

At the same time, the typical Pc1 waves were also observed by the SGO stations on the ground for several hours. As shown in Figure 6, from UTC 21:35 to 24:00, SGO stations recorded continuous pulsations with a central frequency of about 2-3 Hz. In Figure 6, from top to bottom are the observations from SGO stations: Sodankylä (SOD; *L* = 5.3, 64.3°N, 105.6°E, QD), Oulu (OUL; *L* = 4.5, 61.9°N, 104.1°E, QD), and Nurmijärvi (NUR; *L* = 3.4, 57.1°N, 101.2°E, QD) from ~21:00 to 24:00 UT. The wave power of Pc1 pulsations increases monotonically with the decrease of *L* shell values of SGO stations, with the maximum power at NUR station, which is close to the region where CSES observed Pc1 in the Northern hemisphere. Because of the ducting effect of Pc1 waves in the ionospheric waveguide, Pc1 waves are likely to be seen at a long distance away from the source region [e.g., Fujita and Taomao, 1988; Kim et al., 2010]. Since the

boundary of the waveguide is not a perfect conductor, some absorption may happen when waves propagate in the waveguide, resulting in attenuation of the wave power. So, comparing the wave power observed by different ground stations, it is possible to infer the probable location of the wave source. Therefore, in our case, we suggest that the injection source region of the Pc1 waves in the Northern hemisphere should be near (QD-LAT=54 - 56°N, *L*=~ 3.3), where CSES and NUR observed the pulsations, and after incidence on the ionosphere, the waves were ducted toward northeast, observed by the ground stations located at higher latitudes.

3.2 Propagation characteristics of Pc1 waves

Wave polarization is another property that provides information on the wave source and spatial characteristics of wave propagation. According to theoretical studies, the incident LHP Alfven waves in the ionosphere can gradually change to RHP as the waves propagate in the ionosphere away from the injection region [e.g., Fujita and Taomao 1986]. Close to the injection region, the polarization pattern is usually complex, because the waves near the injection source are combined with incident waves and ducting waves [Hayashi et al., 1981; Kim et al., 2010].

We further analyzed the propagation characteristics of Pc1 waves observed by CSES and Swarm satellites in the Northern and Southern hemispheres during the magnetic storm recovery phase. Firstly, we converted the magnetic field into field-aligned coordinates (FAC) and then applied polarization analysis according to the method of Means et al. [1972]. From top to bottom, Figs. 7a-e shows Swarm magnetic field components in FAC (including perpendicular components Br and Ba marked in blue and green and the parallel component Bz marked in red), magnetic wave power spectrum in perpendicular direction and parallel direction, wave normal angle (0° indicates parallel propagation and 90° indicates perpendicular propagation to the background magnetic field), ellipticity (positive indicates RHP and negative indicates LHP). For CSES, electric components in FAC, electric wave power spectrum in perpendicular direction and parallel direction, and field-aligned Poynting flux are also included in Figures 8 and 9.

It can be seen from the Swarm and CSES data in the Southern (Figure 7,8) and Northern hemispheres (Figure 9), that wave normal angles (Figs. 7d, 8g and 9g) predominate below ~ 20°, indicating that Pc1 waves propagated almost parallel to the background magnetic field. Our result is somewhat different from the nightside observations in the ionosphere by Pisa et al. (2015) and Kim et al. (2018), which show the wave normal angles are scattered or have different tendency between two hemispheres. For CSES,

based on the HPM and EFD data, we also calculate the field-aligned Poynting flux of Pc1 waves (shown by Figs. 8i and 9i), which is positive in the Northern hemisphere, negative in the Southern hemisphere, indicating that Pc1 waves observed by CSES propagate along the background magnetic field downward into the ionosphere in the both hemispheres.

Additionally, we find that the waves have dominant perpendicular power, and the parallel power (compressional power) is almost zero (shown at Figs. 7b-c, 8e-f and 9e-f), which means the waves are transverse. The transverse wave is one of the characteristics of the incident wave near the wave injection region [Engebretson et al.,2008; Kim et al., 2010]. The transverse wave also explains why the downward(upward) component in the local North-East-Down(up) coordinates has the minimum wave power, as observed by satellites and ground stations (Figure 2-3, Figure 6). Near the injection region with a geomagnetic latitude of ~55°, the dip angle of the geomagnetic field is about 73°. For a transverse wave, the power projected to the downward direction should be small. We further find the wave normal, electric field vector, background magnetic field are almost lie in the same plane (not shown here) with a deviation less than +/- 8°, which confirms that the incident transverse wave is Alfvénic.

From Figs. 7e, 8h and 9h, the ellipticity of Pc1 waves shows mixed polarization for the waves detected by CSES and Swarm in both hemispheres. To check whether our calculation results truly represent these wave properties, we also use Minimum and Maximum Variance Analysis (MVA) [Sonnerup & Scheible, 1998] to get the MVA hodograph and the wave normal direction (not shown here), which are also consistent with current results. Therefore, it seems that all the Pc1 waves observed by CSES and Swarm have mixed ellipticities and propagate along the background magnetic field.

Discussion

In 1970, Cornwall et al. proposed that during storm recovery phase, the plasmapause expanding into the ring current region can excite EMIC wave. Through simulation, Horne and Thorne et al. [1993] found that the growth rate of EMIC wave inside the plasmapause is obviously lower than that outside the plasmapause, and its peak is near the plasmapause.

To identify the source of the Pc1 waves observed by CSES and Swarm, we use the dynamic plasmasphere model from the Community Coordinated Modeling Center (CCMC) [Pierrard et al., 2008] to obtain the variation of the position of the

plasmapause during this magnetic storm on August 26, 2018 (as shown in Figure 10). The dots correspond to the position of the plasmapause and the red star represents the conjugate location of Pc1 waves observed by CSES in the Southern hemisphere. From 11 to 21 MLT there is a plume rotating with the plasmasphere in the eastward direction. Such plumes are mostly formed during geomagnetic storm recovery phase [Pierrard and Cabrera, 2005]. Meanwhile, the simulation cycle of dynamic plasmasphere model always start at 02 MLT because the plasmas are unstable at post-midnight since the convection electric field has the largest value. Additionally, the simulation does not stop after one full cycle at 02 MLT but continues farther up to 05 MLT showing two plasmapause branches between 02 MLT and 05 MLT and the gaps are caused by the loss of some of the plasma elements at large Kp jumps [Verbanac et al., 2018; Bandic at al., 2019]. Results show that the plasmapause moves outward at about UTC 23:00 on August 27, and the L value reaches about 3 near local time 02:00. Moreover, based on the formula in Carpenter and Anderson [1992] (shown as equation 1), the position of the plasmapause is estimated at about L=2.98. Therefore, we suggest that the possible sources of Pc1 waves are nearly located at the plasmapause, and this is consistent with previous studies, that the outward expansion of the plasmasphere into the ring current during the recovery phase of geomagnetic storms may generate EMIC waves, which propagate along the background magnetic field to the ionosphere, and be observed by multi-ground stations [Wentworth,1964; Cornwall et al., 1970; Russell & Thorne, 1970].

$$\hat{L}_{pp} = 5.6 - 0.46 \times max_{-24,-4} K_p \quad (1)$$

According to the wave analysis performed using CSES and Swarm data, together with ground station observations, we suggest that the satellites are close to the wave injection regions in the Southern and northern hemisphere, during the recovery phase of the storm. The incident waves propagate almost along the background magnetic field, as transvers Alfven waves, which has long been predicted by theoretical studies, although direct observations are rare. However, the ellipticity of the waves shows a complex pattern, which is different from the polarizations of EMIC waves (LHP) in the magnetosphere found by previous works [Fraser et al., 1975a, b; Erlandson et al., 1990]. Theoretical studies predict that EMIC waves trigged near the Earth's magnetic equator propagate toward the ionosphere, changing wave characteristics such as ellipticity and wave normal angle when they pass through multicomponent plasma [Denton, 2018; Johnson & Cheng, 1999; Kim & Johnson, 2016]. The mixed polarization pattern observed in our case might either result from incident waves with complex polarization pattern, or be attributed to the interference between the incident wave and ducting waves in the ionospheric waveguide.

Joint magnetic field and electric field observations onboard CSES provide unambiguous evidence that Pc1 waves propagate downward into the ionosphere in the nearly conjugate ionospheric regions. Although the observations at north and south are temporally separated by about 30 mins, it seems reasonable to infer that the EMIC waves propagate northward and southward from the magnetic equatorial region simultaneously, and wave reflection from the ionosphere is insignificant. Our result is in accord with the CRRES satellite measurements reported by Loto'aniu et al. (2005), which observed that outside a region of about +/-11° MLAT around the equator, the Poynting vectors of the EMIC waves are directed away from the equator along the magnetic field lines.

Pc1 waves sometimes have repetitive wave packet structures, which have been explained by a bouncing wave packet model [e.g., Jacobs and Watanabe, 1964]. According to this model, a wave packet triggered in the equatorial region travels along the magnetic field line, and is reflected between conjugate hemispheres. The Poynting vector is an important parameter for establishing the propagation direction of wave packet energy. CSES observations of Poynting vector in the ionospheric do not seem to support this model.

Conclusion

In this paper, using the simultaneous observations from CSES and Swarm satellites and the ground geomagnetic stations data, we investigated the typical Pc1 waves in the Northern and Southern ionospheric hemispheres. Our principal results are as follows.
1. During the storm recovery phase on Aug. 27, 2018, the typical Pc1 waves were recorded by the SGO stations on the ground for several hours. Meanwhile, the Pc1 waves were detected by the China Seismo-Electromagnetic Satellite (CSES) and Swarm both in Northern and Southern hemispheres in the high latitude post-midnight ionosphere region with a central frequency about 2 Hz.

2. In the field-aligned coordinate system, the power spectrum, ellipticity and normal wave angle, Poynting vector are analyzed. Results show that the satellites observed transverse Alfven waves with mixed polarizations, propagating almost parallel to the background magnetic field downward, which imply the satellites were close to the wave injection region in the ionosphere at about L=3. Attenuation of Pc1 wave power at ground stations with increasing distance from L=3 also supports the idea that CSES observes the wave activity near the injection region.

3. Furthermore, it is also found that the position of the plasmapause calculated by the

CCMC model and the equation of Carpenter and Anderson is almost at *L*=3. Therefore, we suggest the possible sources of waves are near the plasmapause, which is consistent with previous studies that the outward expansion of the plasmasphere into the ring current during the recovery phase of geomagnetic storms may generate electromagnetic ion cyclotron (EMIC) waves. Downward pointing Poynting fluxes measured by CSES at nearly conjugate hemispheres suggest EMIC waves propagate northward and southward simultaneously to the ionosphere at about *L*=3.

Acknowledgments

The work is supported by NSFC grant 41904147, National Key Research and Development Programs of Ministry of Science and Technology of the People´s Republic of China (MOST) (2016YBF0501503, 2018YFC1503501). This research made use of the data from CSES mission, a project funded by China National Space Administration (CNSA) and China Earthquake Administration (CEA). Additionally, thanks to CSES teams for providing CSES HPM and EFD data from website link http://www.leos.ac.cn/, ESA Swarm teams for providing Swarm FGM data from the ftp://Swarm-diss.eo.esa.int/ , and the PI of pulsation magnetometers from Sodankylä Geophysical Observatory(SGO) for providing the geomagnetic pulsation data(https://www.sgo.fi/Data/Pulsation/), and NASA CDA Web (https://cdaweb.sci.gsfc.nasa.gov/index.html/) for providing the OMNI solar wind and magnetic field data, and NASA CCMC Web (https://ccmc.gsfc.nasa.gov/) for providing the plasmapause simulation data.

References

Anderson, B. J., Takahashi, K., Erlandson, R. E., & Zanetti, L. J.: Pc1 pulsations observed by AMPTE/CCE in the Earth's outer magnetosphere, Geophysical Research Letters, 17(11), 1853–1856, https://doi.org/10.1029/gl017i011p01853, 1990.

Anderson, B. J., & Hamilton, D. C.: Electromagnetic ion cyclotron waves stimulated by modest magnetospheric compressions, Journal of Geophysical Research, 98(A7), 11369, https://doi.org/10.1029/93ja00605, 1993.

Anderson, B. J., Denton, R. E., Ho, G., Hamilton, D. C., Fuselier, S. A., and Strangeway, R. J.: Observational test of local proton cyclotron instability in the Earth's magnetosphere, Journal of Geophysical Research: Space Physics, 101(A10), 21527–21543, https://doi.org/10.1029/96ja01251, 1996.

Bandić, M., Verbanac, G., & Pierrard, V.: Relationship between global plasmapause characteristics and plasmapause structures in the frame of interchange instability mechanism. Journal of Geophysical Research: Space Physics. https://doi:10.1029/2019ja026768, 2019.

Bortnik, J., Cutler, J. W., Dunson, C., Bleier, T. E., & McPherron, R. L.: Characteristics of low-latitude Pc1 pulsations during geomagnetic storms, Journal of Geophysical Research: Space Physics, 113(A4), https://doi.org/10.1029/2007ja012867, 2008.

Bossen, M., McPherron, R. L., & Russell, C. T.: A statistical study of Pc 1 magnetic pulsations at synchronous orbit, Journal of Geophysical Research, 81(34), 6083–6091, https://doi.org/10.1029/ja081i034p06083, 1976.

Carpenter, D. L., & Anderson, R. R.: An ISEE/whistler model of equatorial electron density in the magnetosphere, Journal of Geophysical Research, 97(A2), 1097, https://doi.org/10.1029/91ja01548, 1992.

Cornwall, J. M.: Cyclotron instabilities and electromagnetic emission in the ultralow frequency and very low frequency ranges, Journal of Geophysical Research, 70(1), 61–69, https://doi.org/10.1029/jz070i001p00061, 1965.

Cornwall, J. M., Coroniti, F. V. and Thorne, R. M.: Turbulent loss of ring current protons, J. Geophys. Res., 75(25), 4699–4709, https://doi.org/10.1029/JA075i025p04699,1970.

Denton, R. E.: Electromagnetic Ion Cyclotron Wave fields in a Realistic Dipole Field, Journal of Geophysical Research: Space Physics, 123(2), 1208–1223, https://doi.org/10.1002/2017ja024886, 2018.

Engebretson, M. J., Posch, J. L., Westerman, A. M., Otto, N. J., Slavin, J. A., Le, G., Strangeway, R. J. and Lessard, M. R.: Temporal and spatial characteristics of Pc1 waves observed by ST5, Journal of Geophysical Research: Space Physics, 113(A7), https://doi.org/10.1029/2008ja013145, 2008.

Erlandson, R. E., Aggson, T. L., Hogey, W. R., & Slavin, J. A.: Simultaneous observations of subauroral electron temperature enhancements and electromagnetic ion cyclotron waves, Geophysical Research Letters, 20(16), 1723–1726, https://doi.org/10.1029/93gl01975, 1993.

Fraser, B. J.: Polarization of Pc 1 pulsations at high and middle latitudes, Journal of Geophysical Research, 80(19), 2797–2807, doi:10.1029/ja080i019p02797, 1975a.

Fraser, B. J.: Ionospheric duct propagation and Pc 1 pulsation sources, Journal of Geophysical Research, 80(19), 2790–2796, https://doi.org/10.1029/ja080i019p02790, 1975b.

Friis-Christensen, E., Lühr, H. and Hulot, G.: Swarm: A constellation to study the Earth's magnetic field. Earth Planet Sp 58, 351–358, https://doi.org/10.1186/BF03351933, 2006.

Fujita, S., and Tamao, T.: Duct propagation of hydromagnetic waves in the upper ionosphere, 1, Electromagnetic field disturbances in high latitudes associated with localized incidence of a shear Alfvén wave. Journal of Geophysical Research, 93(A12), 14665. https://doi.org/10.1029/ja093ia12p14665, 1988.

Hayashi, K., Kokubun, S., Oguti, T., Tsuruda, K., Machida, S., Kitamura, T., Saka, O.,

Watanabe, T.: The extent of Pc 1 source region in high latitudes, Canadian Journal of Physics, 59(8), 1097–1105, https://doi.org/10.1139/p81-145, 1981.
Horne, R. B., & Thorne, R. M.: On the preferred source location for the convective amplification of ion cyclotron waves, Journal of Geophysical Research, 98(A6), 9233, https://doi.org/10.1029/92ja02972, 1993.
Huang, J., Lei, J., Li, S., Zeren, Z., Li, C., Zhu, X., Yu, W.: The Electric Field Detector (EFD) onboard the ZH-1 satellite and first observational results, Earth and Planetary Physics, 2(6), 469–478, https://doi.org/10.26464/epp2018045, 2018.
Iyemori, T., and Hayashi, K.: PC 1 micropulsations observed by Magsat in the ionospheric F region, Journal of Geophysical Research, 94(A1), 93, https://doi.org/10.1029/ja094ia01p00093, 1989.
Jacobs, J.A., Watanabe, T.: Micropulsation whistlers, Journal of Atmospheric and Terrestrial Physics 26, 825–829, https://doi.org/10.1016/0021-9169(64)90180-1, 1964.
Johnson, J. R., & Cheng, C. Z.: Can Ion Cyclotron Waves Propagate to the Ground? Geophysical Research Letters, 26(6), 671–674, https://doi.org/10.1029/1999gl900074, 1999.
Kim, H., Lessard, M. R., Engebretson, M. J., Lühr, H.: Ducting characteristics of Pc 1 waves at high latitudes on the ground and in space, Journal of Geophysical Research: Space Physics, 115(A9), https://doi.org/10.1029/2010ja015323, 2010.
Kim, E.-H., and Johnson, J. R.: Full-wave modeling of EMIC waves near the He+ gyrofrequency, Geophysical Research Letters, 43(1), 13–21, https://doi.org/10.1002/2015gl 066978, 2016.
Kim, H., Hwang, J., Park, J., Bortnik, J., Lee, J.: Global characteristics of electromagnetic ion cyclotron waves deduced from Swarm satellites, Journal of Geophysical Research: Space Physics, 123, 1325–1336, https://doi.org/ 10.1002/2017JA024888, 2018.
Lin, R. L., Zhang, J. C., Allen, R. C., Kistler, L. M., Mouikis, C. G., Gong, J. C., Liu, L. Q., Klecker, B., Sauvaud, J. A., Dunlop, M. W.: Testing linear theory of EMIC waves in the inner magnetosphere: Cluster observations, Journal of Geophysical Research: Space Physics, 119(2), 1004–1027, http://doi.org/10.1002/2013ja019541, 2014.
Loto'aniu, T. M.: Propagation of electromagnetic ion cyclotron wave energy in the magnetosphere, Journal of Geophysical Research, 110(A7). https://doi.org/10.1029/2004ja010816, 2005.
Lysak, R. L: Propagation of Alfven waves through the ionosphere: Dependence on ionospheric parameters, J. Geophys. Res., 104, 10,017, https://doi.org/10.1029/1999JA900024, 1999.
McCollough, J. P., Elkington, S. R., Usanova, M. E., Mann, I. R., Baker, D. N., Kale, Z. C.: Physical mechanisms of compressional EMIC wave growth, Journal of Geophysical Research: Space Physics, 115(A10), https://doi.org/10.1029/2010ja015393, 2010.

Means, J. D.: Use of the three-dimensional covariance matrix in analyzing the polarization properties of plane waves, Journal of Geophysical Research, 77(28), 5551–5559, https://doi.org/10.1029/ja077i028p05551, 1972.

Merayo, J. M. G.: The Swarm Vector Field Magnetometer (VFM): instrument commissioning & performance assessment, 3rd Swarm Science Meeting, Copenhagen, Denmark, 19-20 June 2014.

Olson, J. V., & Lee, L. C.: Pc1 wave generation by sudden impulses, Planetary and Space Science, 31(3), 295–302, https://doi.org/10.1016/0032-0633(83)90079-x, 1983.

Park, J., Lühr, H., and Rauberg, J.: Global characteristics of Pc1 magnetic pulsations during solar cycle 23 deduced from CHAMP data, Annales de Geophysique, 31(9), 1507–1520, https://doi.org/10.5194/angeo-31-1507-2013, 2013.

Pierrard, V., and Stegen: A three-dimensional dynamic kinetic model of the plasmasphere, J. Geophys. Res., 113, A10209, https://doi.org/10.1029/2008JA013060, 2008.

Píša, D., Parrot, M., Santolík, O. and Menietti, J. D.: EMIC waves observed by the low-altitude satellite DEMETER during the November 2004 magnetic storm, J. Geophys. Res. Space Physics, 120, 5455–5464, https://doi.org/10.1002/2014JA020233, 2015.

Russell, C. T., and Thorne, R. M.: on the structure of the inner magnetosphere, Cosmic Electrodynamics, Vol. 1, p. 67 – 89, 1970.

Sonnerup, B. U. O., & Scheible, M.: Minimum and maximum variance analysis, Chap. 1. In G. Paschmann & P. W. Daly (Eds.), Analysis methods for multi-spacecraft data, No. SR-001 in ISSI Scientific Reports (pp. 185–220). Noordwijk, Netherlands: ESA Publications Division, 1998.

Usanova, M. E., Mann, I. R., Bortnik, J., Shao, L., Angelopoulos, V.: THEMIS observations of electromagnetic ion cyclotron wave occurrence: Dependence on AE, SYMH, and solar wind dynamic pressure, Journal of Geophysical Research: Space Physics, 117(A10), https://doi.org/10.1029/2012ja018049, 2012.

Wentworth, R. C.: Enhancement of hydromagnetic emissions after geomagnetic storms, J. Geophys. Res., 69(11), 2291–2298, https://doi.org/10.1029/JZ069i011p02291, 1964.

Verbanac, G., Bandić, M., Pierrard, V., & Cho, J.: MLT Plasmapause Characteristics: Comparison Between THEMIS Observations and Numerical Simulations. Journal of Geophysical Research: Space Physics. https://doi:10.1002/2017ja024573, 2018.

Zhou, B., Yang, Y. Y., Zhang, Y. T., Gou, X. C., Cheng, B. J., Wang, J. D., and Li, L.: Magnetic field data processing methods of the China Seismo-Electromagnetic Satellite, Earth Planet. Phys., 2(6), 455–461, https://doi.org/10.26464/epp2018043, 2018.

Zhou, B., Cheng, B. J., Gou, X.C., Li, L., Zhang, Y. T., Wang, J. D., Magnes, W., Lammegger, R., Pollinger, A., Ellmeier, M., Xiao, Q., Zhu, X. H., Yua, S. G., Yang, Y. Y. and Shen, X. H.:

First in-orbit results of the vector magnetic field measurement of the High Precision Magnetometer onboard the China Seismo-Electromagnetic Satellite, Earth Planets Space 71, 119, https://doi.org/10.1186/s40623-019-1098-3, 2019.

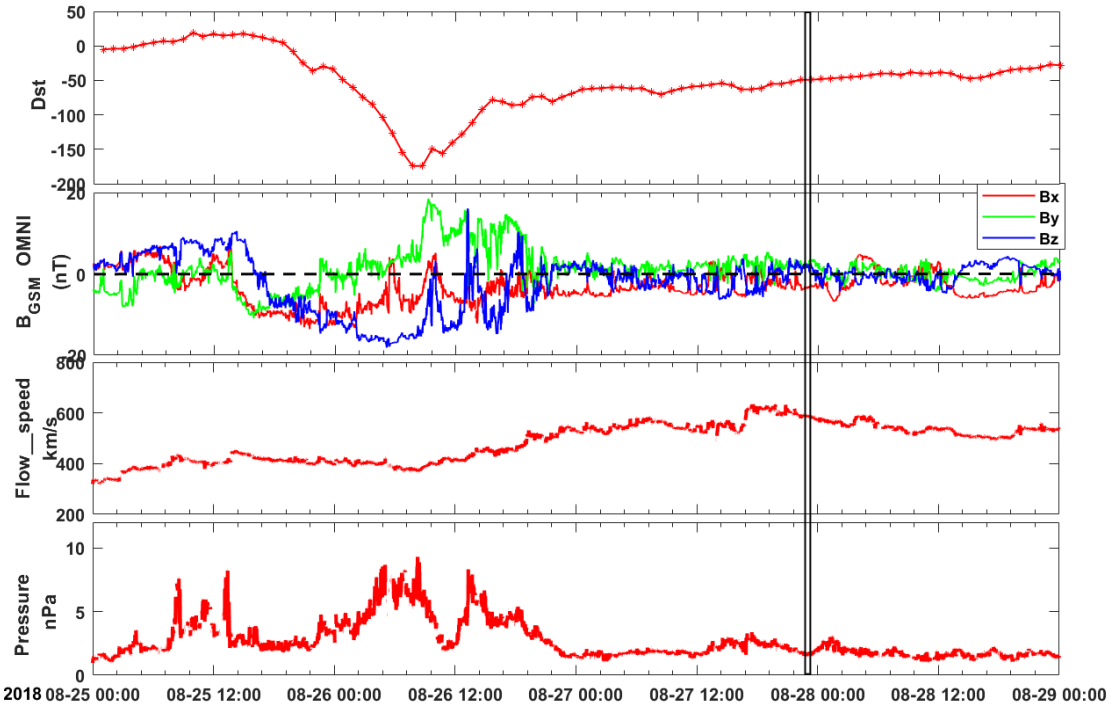

Figure 1. The solar wind conditions and geomagnetic index from Aug. 25 to 29, 2018. From top to bottom: Dst index, interplanetary magnetic field, solar wind speed and solar wind dynamic pressure, respectively. The occurrence of Pc1 waves is marked by the black box.

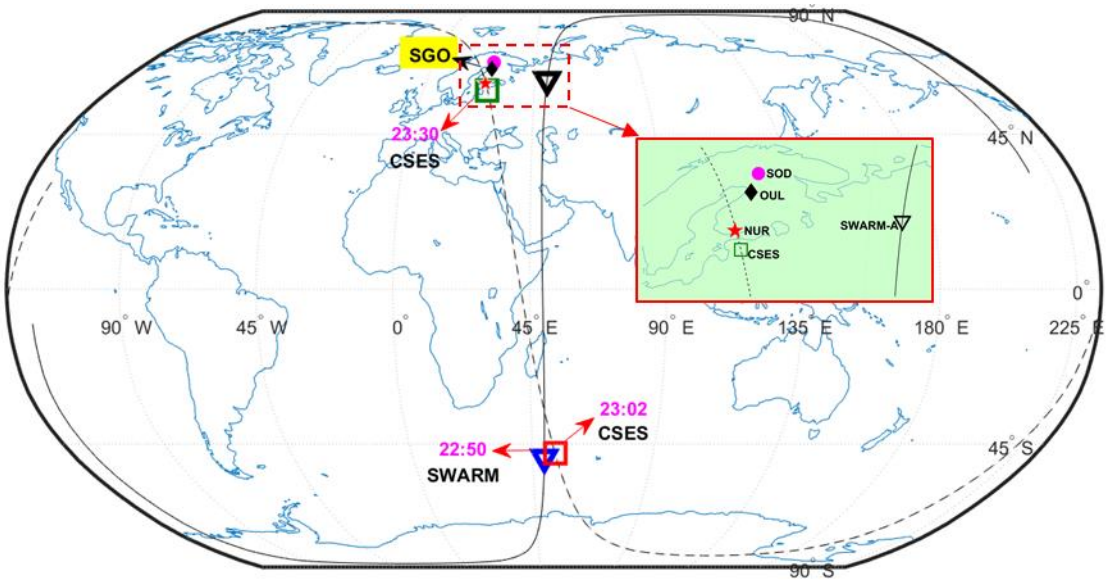

Figure 2. The locations of Pc1 waves observed by CSES (squares) and Swarm (triangles) satellites. The pentagram, rhombus and circle represent three the SGO stations:

Nurmijärvi (NUR; *L* = 3.4, 57.1°N, 101.2°E, QD), Oulu (OUL; *L* = 4.5, 61.9°N, 104.1°E, QD), and Sodankylä (SOD; *L* = 5.3, 64.3°N, 105.6°E, QD), respectively. The black dotted and solid lines denote the trajectories of CSES and Swarm-A satellites, respectively and the red arrows represents three Pc1 wave observations.

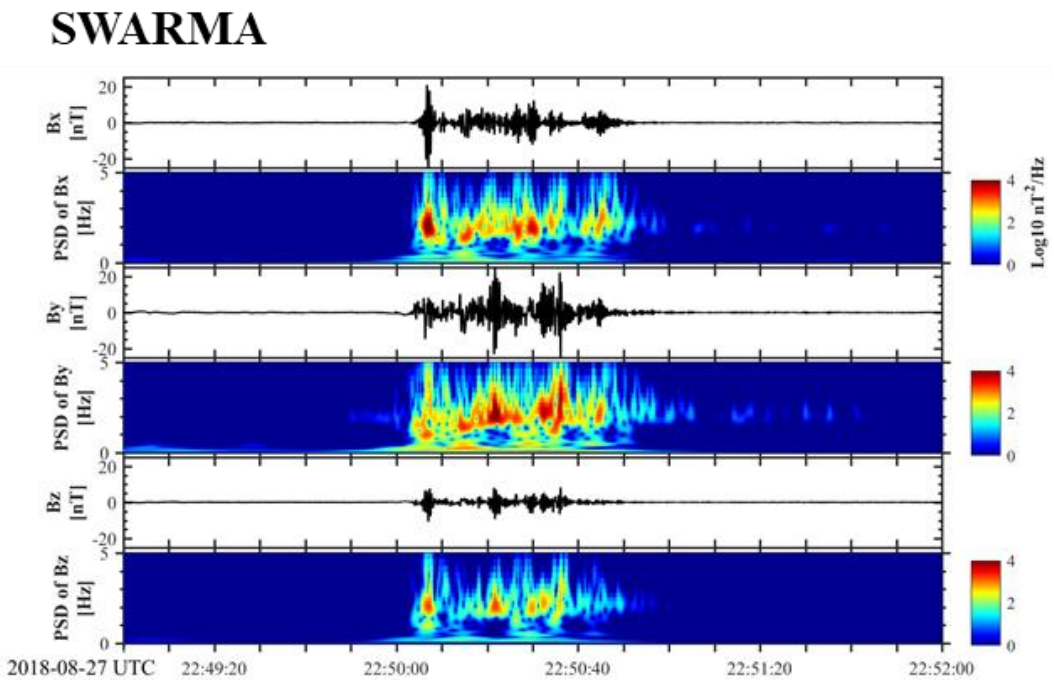

Figure 3. The power spectral densities (PSDs) of the magnetic fields in the local North-East-Down coordinates during the Pc1 wave period (UTC 22:50-22:51) observed by Swarm -A.

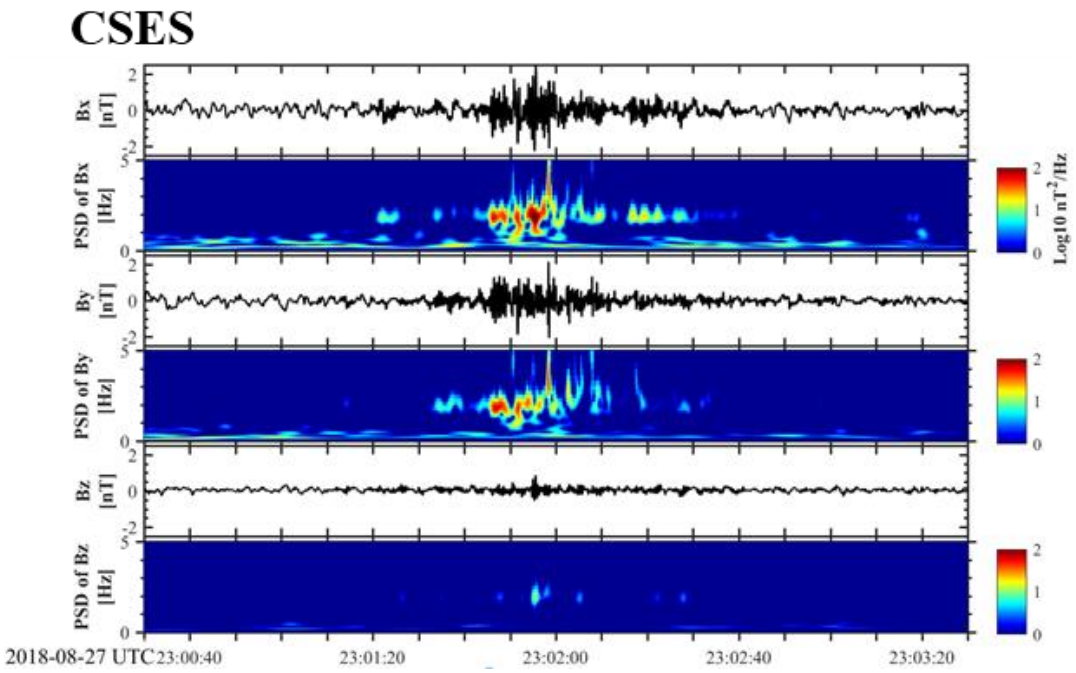

Figure 4. The power spectral densities (PSDs) of the magnetic fields in the local North-East-Down coordinates during the Pc1 wave period (UTC 23:01-23:02) observed by

CSES.

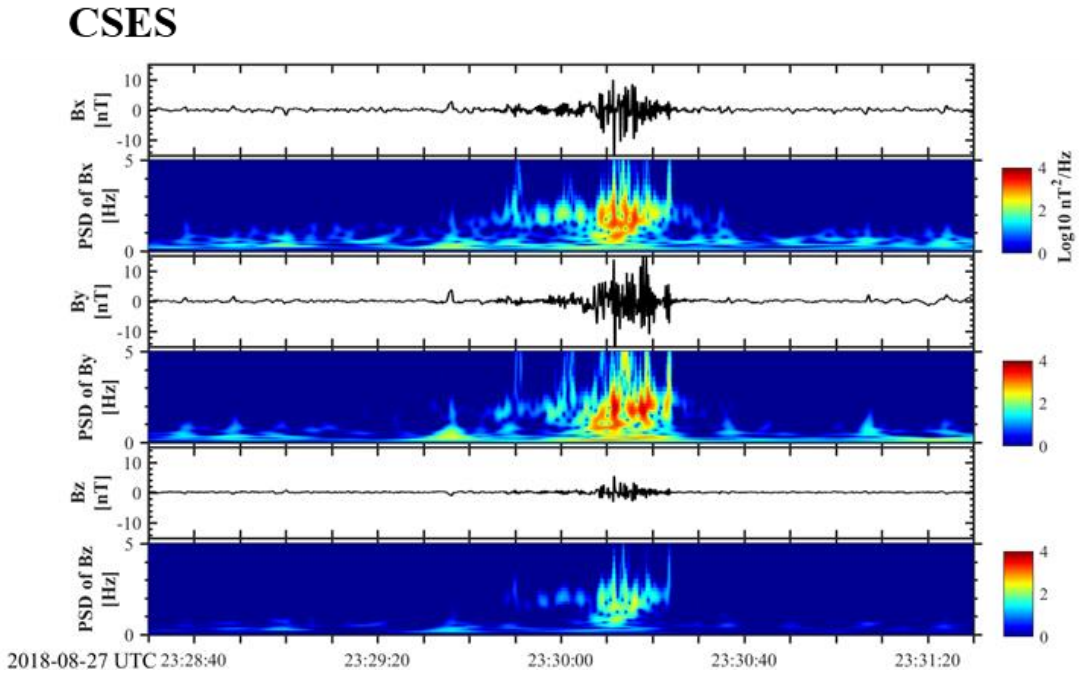

Figure 5. The power spectral densities (PSDs) of the magnetic fields in the local North-East-Down coordinates during the Pc1 wave period (UTC 23:30-23:31) observed by CSES.

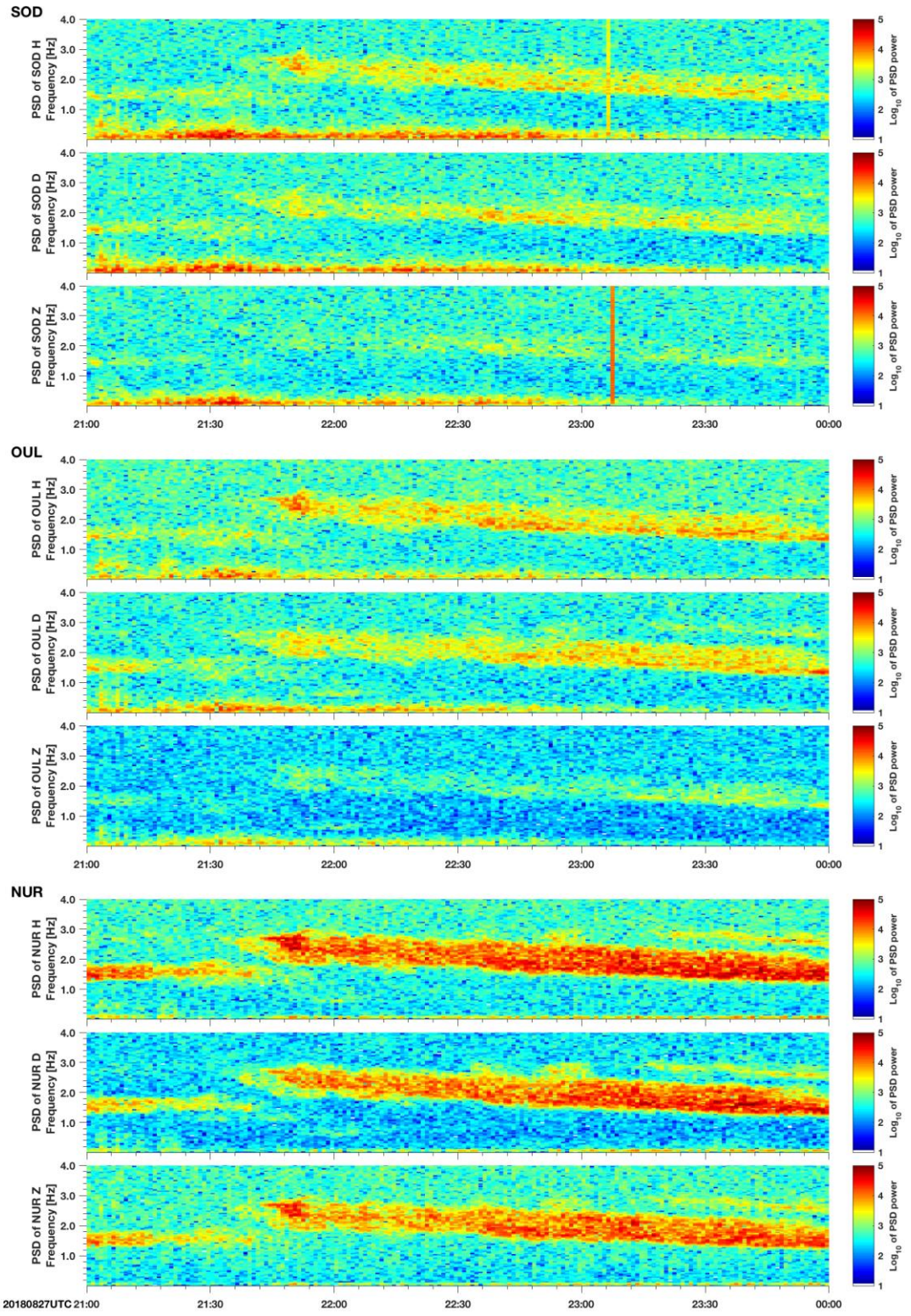

Figure 6. The power spectral densities (PSDs) of the magnetic fields in the local North-East-Up coordinates during the Pc1 wave period (UTC 21:35-24:00) observed by SGO ground stations at different *L* shell values.

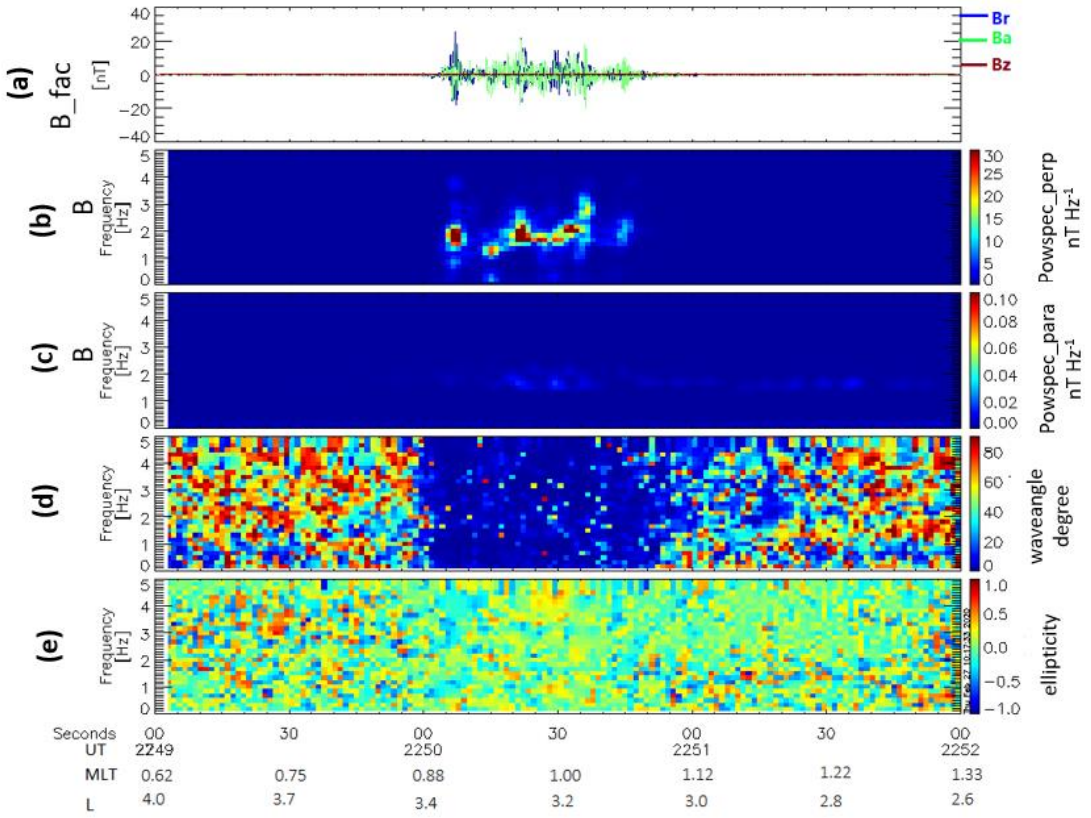

Figure 7. The wave propagation and polarization features of the Pc1 waves observed by Swarm. From top to bottom, (a) magnetic field components (including perpendicular components Ba and Br marked in blue and green, parallel component Bz marked in red), (b) wave power spectrum in perpendicular and (c) parallel directions, (d) wave normal angle and (e) ellipticity computed by wave vector analysis of Means [1972]. (positive indicates right-handed polarization and negative indicates left-handed polarization).

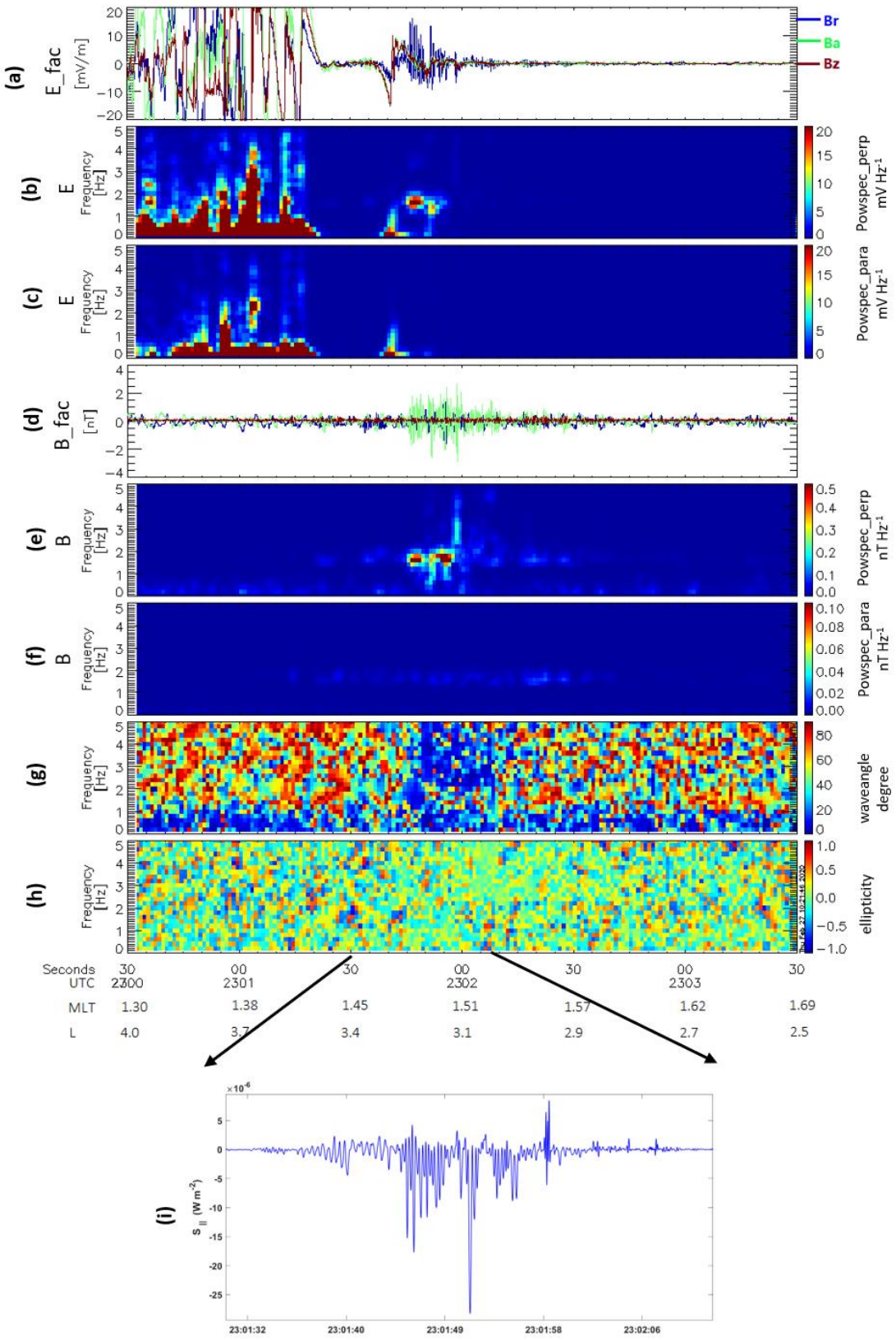

Figure 8. The wave propagation and polarization features of the Pc1 waves observed by CSES in the Southern hemisphere. From top to bottom, (a) electric field components (including perpendicular components Ea and Er marked in blue and green, parallel component Ez marked in rad), (b) electric wave power spectrum in perpendicular and

(c) parallel directions; (d) magnetic field components (including perpendicular components Ba and Br marked in blue and green, parallel component Bz marked in rad), (e) wave power spectrum in perpendicular and (f) parallel directions, (g) magnetic wave normal angle and (h) ellipticity, (i) the field-aligned Poynting fluxes.

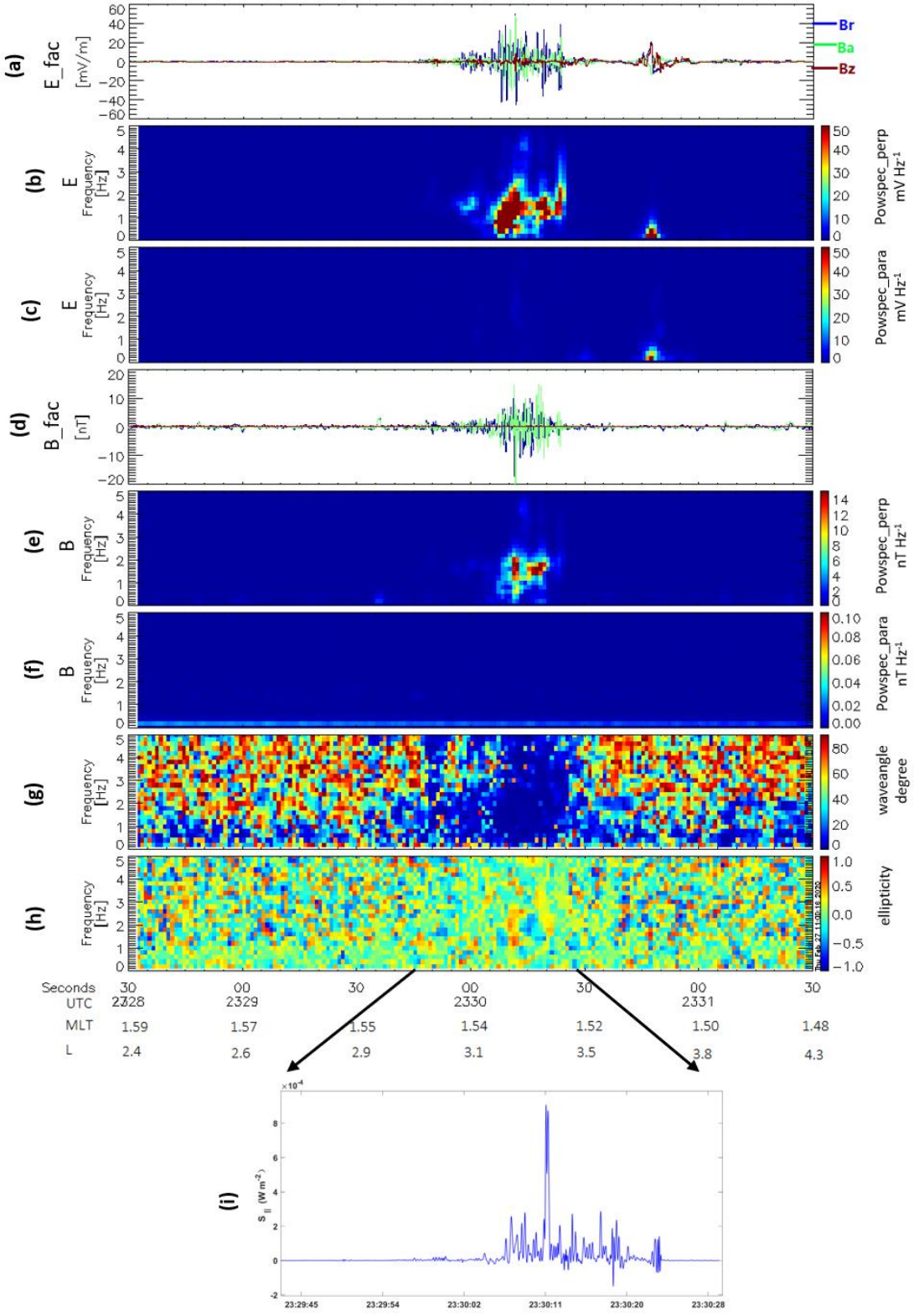

Figure 9. The wave propagation and polarization features of the Pc1 waves observed by CSES in the Nothern hemisphere, same format as Figure 8.

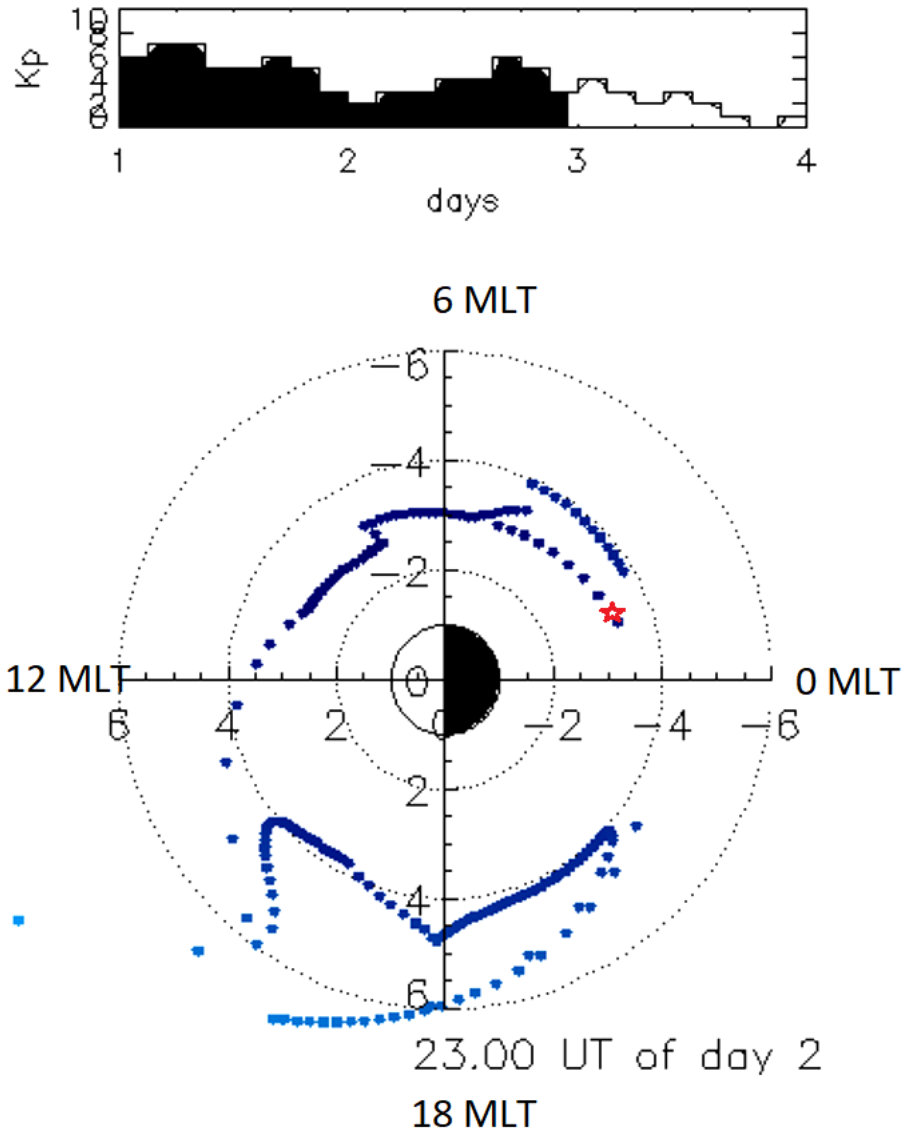

Figure 10. The Kp index (upper) and the simulated plasmapause location (lower) in the geomagnetic equatorial plane marked by blue dots at UTC 23:00 on August 27, 2018 from CCMC Web. The red star represents the conjugate location of Pc1 waves observed by CSES in the Southern hemisphere.